Received ; | Revised ; | Accepted
DOI: xxx/xxxx

ARTICLE TYPE

Investigation of wind turbine wake superposition models using Reynolds-Averaged Navier-Stokes simulations

Christopher Vogel* | **Richard Willden**

Department of Engineering Science, University of Oxford, Oxford OX1 3PJ, United Kingdom

Correspondence
*Christopher Vogel, Department of Engineering Science, University of Oxford, Oxford OX1 3PJ, United Kingdom. Email: christopher.vogel@eng.ox.ac.uk

Summary

It is well accepted that the wakes created by upstream turbines significantly impact on the power production and fatigue loading of downstream turbines, and that this phenomenon affects wind farm performance. Improving the understanding of wake effects and overall efficiency is critical for the optimisation of layout and operation of increasingly large wind farms. In the present work, the NREL 5MW reference turbine was simulated using blade element embedded Reynolds-Averaged Navier- Stokes computations in sheared onset flow at three spatial configurations of two turbines at and above rated flow speed to evaluate the effects of wakes on turbine performance and subsequent wake development. Wake recovery downstream of the rearward turbine was enhanced due to the increased turbulence intensity in the wake, although in cases where the downstream turbine was laterally offset from the upstream turbine this resulted in relatively slower recovery. Three widely-used wake superposition models were evaluated and compared to the simulated flow-field data. It was found that when the freestream hub-height flow speed was at the rated flow speed, the best performing wake superposition model varied depending according to the turbine array layout. However, above rated flow speed where the wake recovery distance is reduced, it was found that linear superposition of single turbine velocity deficits was the best performing model for all three spatial layouts studied.

KEYWORDS:
computational fluid dynamics, blade element model, Reynolds-Averaged Navier-Stokes simulation, wind turbine wake

1 | INTRODUCTION

The size of wind turbines, and the number of turbines in wind farms, has grown significantly over the past few decades as part of the transition towards increased electricity production from renewable energy sources. It has been observed that there are significant power losses when turbines operate in the wake of upstream turbines, with a reduction in time-averaged power on the order of 10-20%[1]. The reduction in power is the

consequence of a number of factors, including inter-turbine spacing and wind direction [2]. Turbines operating in the turbulent wakes of upstream turbines experience lower average flow speeds, and hence reduced power production, and also encounter increased flow unsteadiness, leading to higher fatigue loads. Consequently, it has become increasingly important to understand the aerodynamic interactions that arise between turbines in wind farms. These interactions can be particularly important in the offshore environment, where the low levels of ambient turbulence and the lack of topographical features can result in turbine wakes persisting for many rotor diameters downstream.

Modelling wind turbine wakes within farms is challenging because the wakes evolve and merge with neighbouring wakes in a flow that is different to the freestream flow. Wind turbine wakes are often characterised in terms of two regions: the near wake, and the far wake. The near wake region starts immediately downwind of the turbine, and extends 2-4 rotor diameters, d, downstream, depending on the turbulence level. The flow in the near wake region is complex and strongly influenced by the rotor geometry through the propagation and evolution of the blade root and tip vortices, the strength of which also depends on the operation of the device [3]. There are large gradients of static pressure and streamwise velocity in the near wake region, and the ambient and rotor blade-induced turbulence acts to transport momentum towards the centre of the wake [4]. Rotor geometry only indirectly affects the far wake region, which is characterised by increased turbulence levels and a streamwise velocity deficit. In this region the wake is fully developed and self-similar, although affected by the presence of the ground and vertical shear profile [2]. Additionally, it has been shown that the manner in which the turbines are operated, i.e. the turbine thrust, plays an important role in how the wake develops and hence on the significance of wake interactions. For example, Adaramola and Krogstad [5] showed in experimental testing that reducing the thrust of the upstream turbine could result in higher overall farm power due to the increase in performance achieved by the downstream turbine.

The high Reynolds numbers that arise in wind turbine wake modelling mean that the underlying physics spans a wide range of spatial and temporal scales, which presents a significant challenge in the modelling of wind turbine wakes. Increases in computer power have allowed detailed Computational Fluid Dynamics (CFD) investigations using Reynolds-Averaged Navier-Stokes (RANS) models [6,7,8] or Large Eddy Simulations (LES) [9,10,11] to be used to simulate turbine wakes. The number of turbines that can be simulated is constrained by the choice of turbine representation; the mesh resolution required to simulate blade boundary layers on turbines is orders of magnitude greater than that using simplified representations such as actuator disks. Blade boundary layer flows are important for studying the near wake region, but it may be sufficient to use simplified turbine representations when considering interactions in the far wake region as blade scale 3D flow phenomena dissipate relatively quickly within the near wake region.

Despite the progress that has been made in the numerical simulation of wind turbine wakes, fast engineering models are still required to evaluate the large number of design cases and operating conditions in wind farms. The accuracy of such models is limited because lower order models cannot capture all the complex 3D flow phenomena that arise in wakes. Wind farm design tools typically predict wake evolution based on single turbine wake models, which are then used with wake combination methods to determine the profile of the combined wake [12,13]. The emergent flow physics that arises as wakes evolve and combine with neighbouring wakes is not captured in current wake superposition models, which are based on simple mathematical models. Hence, it has been found that the accuracy of engineering wind farm models is limited under some flow conditions. For example, Machefaux et al. [12] compared LES CFD simulation of two actuator disks inline with the mean flow to the predictions of

four wake superposition models. This was extended by Gunn et al.[13] to consider the effect of the downstream turbine being laterally offset behind the first device, which was compared to both RANS CFD simulation and experimental testing. Different wake superposition models were found to perform better for the different spatial configurations. The present study extends this work further to consider the effect of turbine layout and operation on how the combined wakes merge and evolve.

2 | COMPUTATIONAL MODEL

The turbine used in this study was the three-bladed variable speed 5MW reference wind turbine designed by the National Renewable Energy Laboratory (NREL)[14]. The turbine has a diameter $d = 126$ m, and a hub height of 90 m, and has a rated flow speed of 11.4 ms^{-1}. The blade chord tapers between 4.6 m at the root to 1.4 m at the tip, transitioning smoothly between the DU99-W-405 to DU93-W-210 to NACA64-618 aerofoil sections between 20% and 70% of the rotor radius R, continuing with the NACA64-618 aerofoil section outboard to the tip. The aerofoil lift and drag polars were drawn from Jonkman et al.[14], which include corrections for 3D flow effects including rotational stall delay and development.

2.1 | Numerical model

Numerical simulations were performed as steady computations using the finite volume software ANSYS Fluent 15.0, solving the 3D incompressible RANS equations. The SIMPLE algorithm was adopted for pressure-velocity coupling, and a second-order upwind scheme was employed for the convective terms. A RANS-embedded blade element actuator disk (BE-AD) method was used to represent the turbines, implemented as a set of users defined functions in Fluent imposed on a zero-thickness fan internal boundary condition, which allow static pressure jumps and swirl velocities to be imposed on the flow to represent the effect of the turbines without requiring resolution of the blade surfaces.

BE-AD models divide the rotor swept area into a number of independent concentric annuli, and use blade element theory (e.g.[15]) to determine the radially varying lift and drag forces that arise from the local flow conditions at the rotor plane based the specified rotor geometry (twist and solidity) and two-dimensional aerofoil data. The local solidity ratio $\sigma(r) = N_B c(r)/2\pi r$, where N_B is the number of blades and $c(r)$ is the blade chord at radius r. The static pressure jump imposed across the fan boundary condition is determined as

$$\Delta p = \frac{1}{2}\rho V^2 \sigma(r) \left(C_l \cos\phi + C_d \sin\phi\right) \tag{1}$$

where ρ is the fluid density, the incident flow $V = \sqrt{u_x^2 + (\Omega r - u_\theta)^2}$ is resolved from the computed local axial and tangential velocities, u_x and u_θ respectively given the rotational speed Ω. The lift and drag coefficients, C_l and C_d are specified for a two-dimensional aerofoil as functions of angle of attack determined from the incident flow angle $\phi = \arctan\left(u_x/\Omega r - u_\theta\right)$. The imposed swirl velocity downstream of the disk is given as

$$u_\theta = -\frac{V^2 \sigma(r) \left(C_l \sin\phi - C_d \cos\phi\right)}{2u_x} \tag{2}$$

Consistent with most analytical blade element momentum theory models, it is assumed that the swirl component at the disk plane is half that of its downstream value. The Prandtl tip loss model[16] was implemented to account for discrete blade effects as a tip-loss factor $F(r)$ applied to u_x.

$$F = \frac{2}{\pi} \arccos\left(\exp \frac{N_B\,(1 - R/r)}{2 \sin\phi}\right) \tag{3}$$

The rotor thrust and torque are determined by resolving and integrating the lift and drag across each annulus.

The BE-AD concept has been widely used as a computationally efficient method of representing the effects of turbines in wind and tidal flows[17,18,19,20,21,22]. One difference between different implementations is whether equations (1) and (2) use azimthually averaged values of u_x and u_θ on each annulus, or whether local (radially and azimuthally varying) values of u_x and u_θ are used. The former case (e.g.[23,20,21]) is closer to traditional analytical BEM models where rotor thrust and torque are azimuthal averages, whereas the later approach (e.g.[18,19]) seeks to account for the effect that variations in local flow speed, perhaps due to a vertical velocity profile, have on blade forces around the azimuth. The RANS BE-AD method employed here is an extension of that which has been used in tidal/marine applications[17], and uses local values of u_x and u_θ.

2.1.1 | Turbulence model

Turbulence has a very significant impact on the evolution of wind turbine wakes. Resolution of the tip vortex and the production of small scale turbulence along the blades using rotor-resolving models and careful turbulence modelling is important to accurately capture the dynamics of the near wake region ($\leq$2-3d downstream)[24,23]. However the impacts of rotor geometry is indirect in the far wake region and characterised by reduced axial flow speed and increased turbulence intensity[24], and lower fidelity turbine and turbulence models can be sufficiently accurate.

High-fidelity turbulence modelling approaches, such as Large Eddy Simulation (LES), separate turbulent motions into resolved and unresolved components, spatially averaging turbulent motions below the scale of the computational grid. At the large Reynolds numbers typical of flows in wind farms, the computational expense of LES is high which has limited its uptake to date and means that RANS simulations are an attractive choice for large scale problems. Two-equation turbulence models, based on the eddy viscosity concept, have been widely applied as a relatively cheap method for turbulence modelling in the RANS equations.

One of the limitations of the standard formulations of the $k-\epsilon$ and $k-\omega$ models is that they over predict the production of turbulent kinetic energy k in regions of adverse pressure gradients[25]. Depending on the ambient turbulence level, this usually results in underestimation of the wake deficit as well as errors in the prediction of turbulence energy and dissipation quantities[26,7,20]. Modifications have been proposed to enhance turbulence dissipation close to the rotor in the $k-\epsilon$[27] and $k-\omega$[28] frameworks, or by modifying model constants[26] in order to better match observed wake characteristics. Alternatively, additional terms have been added to $k-\epsilon$ equations in order to provide spatial control over the eddy viscosity to achieve better comparison with observed wakes, for example the $k-\epsilon-f_P$ model[7].

The $k-\omega$ Shear Stress Transport (SST) model was developed by Menter[25] and combines the $k-\omega$ and $k-\epsilon$ models as a function of wall distance, as well as introducing an additional model for the transport of principal turbulent stresses. The formulation proposed by Menter was tailored for

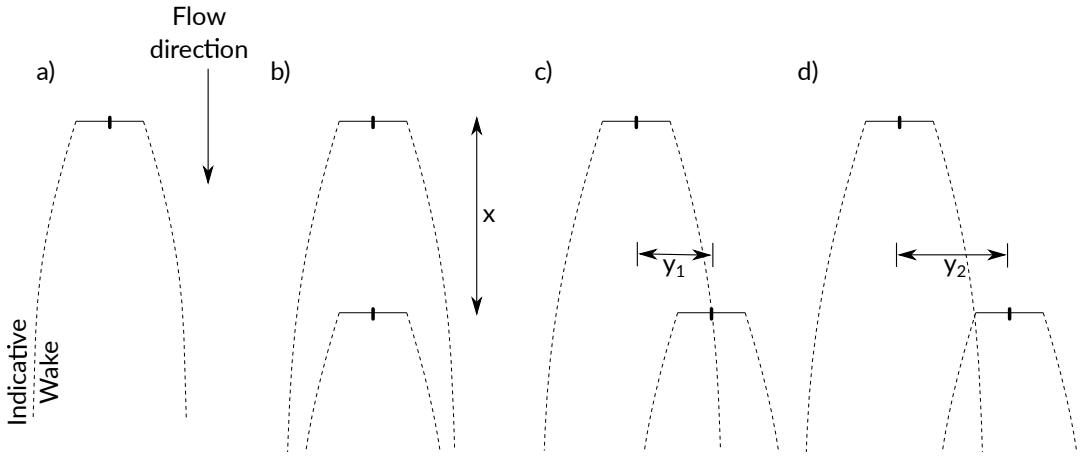

FIGURE 1 Plan view of the single (a) and multi-turbine (b-d) layout configurations investigated in this study. The streamwise spacing $x = 8d$, and the lateral spacings $y_1 = 1d$ and $y_2 = 1.75d$. The turbine diameter is $d = 126$ m.

flows with streamwise pressure gradients and separating flows as encountered in wind turbine applications, and limits the eddy viscosity in regions of high turbulence production. For full model details see [25].

Wake predictions using modified $k-\epsilon$ and the $k-\omega$ SST turbulence have been shown to be a significant improvement over the standard models and compare well to experimental and LES wakes [29,20,21,30]. An advantage of the $k-\omega$ SST model in particular is that the formulation presented by Menter [25] performs well for wake studies using the standard model coefficients, avoiding the need for calibration of model parameters for each application. Hence, the $k-\omega$ SST turbulence model has become increasingly popular for wind and tidal turbine applications [15,29,20,22,31,32], and is employed in this study.

2.2 | Computational setup

Three spatial configurations of two turbines were investigated, as shown in Figure 1. These layouts were selected to examine the performance of single turbine wake superposition models in interacting and overlapping configurations. The streamwise spacing between the upstream and downstream turbines was 8d, and three lateral offsets for the downstream turbine were considered such that the rotor was inline with the upstream rotor, approximately half inside the wake of the upstream rotor, and just outside the wake of the upstream rotor; $y = 0d$, 1d, and 1.75d respectively. A suite of computations were also performed to evaluate the wake development behind a single rotor.

The upstream turbine was centred at $x = y = z = 0$, and the computational domain extended 5d upstream and 20d downstream of the rotor. The downstream turbines were centred at $x = 8d$, $y = 0d$, $y = 1d$, and $y = 1.75d$, and an elevation of $z = 0$. The domain was 9d in width and height, with the floor of the domain at $z = -10/7d = -90$ m. The rotor hub, an ellipsoid of length $d/10 = 12.6$ m and radius 1.5 m was included in the simulations, but the support towers were neglected. Symmetry boundary conditions were applied to the lateral walls of the domain, and a pressure outlet on the downstream boundary. A steady, streamwise flow was introduced at the inflow boundary with a hub-height flow speed of $u_0 = 9.0$ ms^{-1}, which corresponds to Region 2 control of the NREL reference turbine which seeks to maximise power capture [14]. The inlet

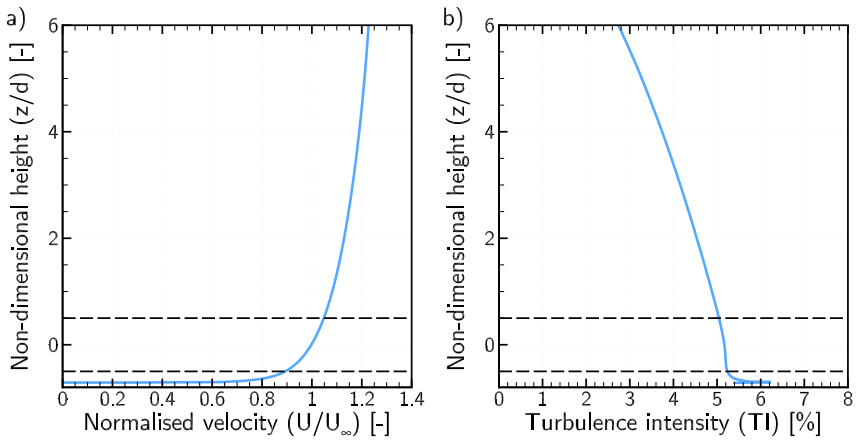

FIGURE 2 Vertical profiles of streamwise flow speed normalised by the hub-height velocity (a) and turbulence intensity (b) in the simulated domain. Dashed lines at $z/d = \pm 0.5$ indicate the vertical position of the turbines.

velocity, turbulent kinetic energy and dissipation profiles corresponded to the freestream velocity profile that develops in the simulated domain in the absence of turbines following [33]. The vertical velocity shear profile was sustained by introducing a constant shear stress to the bottom wall of the computational domain, which resulted in a velocity shear and a turbulence profile across the rotor swept area, following Gunn et al. [13]. The wall shear stress parameter was adjusted to achieve a hub height ambient turbulence intensity representative of offshore conditions of approximately 5.5% at the rotor plane [12]. The resulting vertical profiles of flow speed and turbulence intensity are shown in Figure 2. Note that turbulence intensity, TI, is normalised on the inlet hub-height flow speed, and is defined as

$$TI = \frac{1}{u_0}\sqrt{\frac{2}{3}k} \tag{4}$$

where k is turbulent kinetic energy.

Three mesh resolutions were considered. Following previous experience, a baseline mesh for the single turbine domain was created with an element size of approximately $d/100$ in the regions close to the rotors, resulting in about 7000 elements on the face of the actuator disk. The high density region projected $d/2$ upstream and 10d downstream of each rotor in order to capture the device wakes. Ten prism layers were grown from the domain floor to the bottom edge of the rotor disk to resolve the bottom of the shear profile, and an unstructured mesh was used to fill the remainder of the computational domain. Two further meshes were created, a coarse mesh, where elements were scaled by 1.5, and a fine mesh with a scaling of 0.5.

The effect of mesh resolution on integrated turbine performance characteristics, the power and thrust coefficients, is detailed in Table 1. Differences between the baseline and fine mesh were no greater than 0.2%, whereas differences around 4% were observed C_P and C_T using the coarse mesh, which was affected particularly by the lack of resolution of the effects of tip-losses towards the outboard sections of the rotor. Figure 3 compares the streamwise variation in normalised hub-height velocity for the three meshes. Differences between the baseline and fine meshes are small and within 0.5% at all locations, whereas the over-prediction of thrust in the coarse mesh results in a large wake deficit immediately downstream of the turbine. The velocity deficit recovers more quickly due to coarser mesh being more dissipative. The baseline mesh was concluded

TABLE 1 Effect of mesh resolution on integrated turbine power C_P and thrust C_T coefficients.

Mesh	λ	C_P	C_T
Baseline	8.5	0.53	0.88
Fine	8.5	0.53	0.88
Coarse	8.5	0.51	0.92

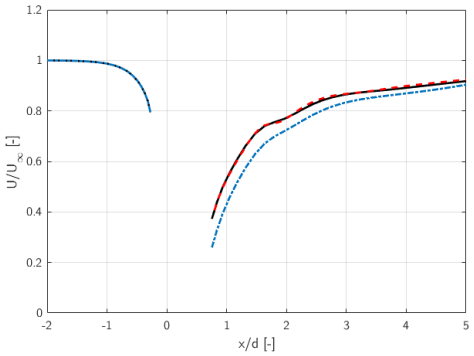

FIGURE 3 Streamwise variation in normalised hub-height velocity U_x/U_∞ predicted with the baseline (black dash), fine (red) and coarse (blue dot-dash) meshes. The turbine nacelle lies between $-0.25 \leq x/d \leq 0.5$

to provide appropriate accuracy at an acceptable computational cost. Solid surfaces in the final mesh had y^+ values in the wall-modelling range (80-170). Comparisons between appropriately-resolved RANS simulations and experimental data have demonstrated very good agreement, with differences less than 7% in point flow field measurements and similar accuracy with prediction of rotor thrust and power coefficients [34].

2.3 | Turbine control

In the first suite of simulations, the rotational speed, ω, of the rotors was adjusted in order to match the rotor aerodynamic torque, $Q_{aero} = P/\omega$, with the 'generator' torque, $Q_{gen} = k\omega^2$, where P is the instantaneous power of the turbine. The mode gain constant, k, is a property of the turbine that was established from single rotor simulations in which ω was varied in order to determine the maximum power coefficient, i.e. $k = P|_{C_P max}/\omega^3$. The angular acceleration of the turbine can be expressed

$$\dot{\omega} = \frac{1}{J}\left(Q_{aero} - Q_{gen}\right) \tag{5}$$

where J is the rotational inertia of the rotor blades [35]. The rotational inertia acts as a damping factor on $\dot{\omega}$ to ensure steady simulations as the NREL 5MW reference rotor is not a physical turbine, and thus its precise value is not important. When the generator torque is too high, the rotational speed of the turbine is reduced to obtain maximum achievable power, whereas when the torque is too low, the rotational speed of the turbine is increased. Above rated flow speed the rotational speed is assumed constant and equal to that at the rated flow speed.

A number of simulations were performed such that the turbines were operating above rated flow speed. Rated power is maintained by pitch to feather control of the blades, for which a similar control strategy as for rotational speed was adopted

$$\dot{\beta} = \frac{1}{\epsilon}\left(P - P_R\right) \tag{6}$$

where β is the blade pitch angle, ϵ is a gain constant, and P_R is the rated power of the turbine. Thus, if instantaneous power is above rated $\dot{\beta}$ is positive resulting in an increase of the geometric pitch of the blades, i.e. pitch to feather. In the absence of further information about the control strategy of the reference turbine, the value of ϵ was chosen to ensure fast and stable convergence of the blade pitch angle.

3 | WAKE SUPERPOSITION MODELS

This study investigates the wake that develops behind three spatial arrangements of two identical wind turbines, as shown in Figure 1. The predictive ability of widely used wake superposition models is evaluated through the comparison of the velocity incident on a hypothetical third wind turbine located 8d downstream of the first two. The models are benchmarked against the RANS CFD simulations described in Section 2. Although only two wind turbine wakes are considered in this study, the superposition models can in principle be extended to consider the merging of n wind turbine wakes. There are however practical limitations to the use of superposition models within large wind farms, in particular for linear superposition of a large number of wakes which can result in non-physical predictions of reversed flow.

The velocity in the wake at hub-height, $u_w(x, y)$, is normalised relative to the hub-height velocity, u_0, 2.5d upstream of the relevant turbine:

$$\hat{u} = \frac{u_w}{u_0} \tag{7}$$

where the magnitude of the wake velocity u_w varies according to the superposition model used. The single turbine wake velocity used in the superposition models is determined from the single turbine RANS CFD simulations.

3.1 | Largest deficit

In the largest deficit superposition model it is assumed that the wake at a particular spatial location is entirely determined as the largest magnitude single turbine wake deficit of all upstream turbines at that point and that all the upstream wakes develop and propagate independently. Hence the single turbine wakes are all determined for the same far upstream flow speed and turbulence intensity conditions. The largest deficit superposition method has been used for example by Larsen et al.[36] in wind farm models including wake meandering. The velocity deficit is calculated as

$$\hat{u}\left(x, y\right) = \min\left(\hat{u}_i\left(x, y\right)\right) \quad \forall i \in (1, n) \tag{8}$$

3.2 | Linear superposition

Linear superposition models, such as that adopted by Lissaman[37], assume that the combined wake deficit at a location corresponding to the (hypothetical) $(n+1)^{th}$ turbine is the result of linear superposition of the n upstream wakes. Each upstream wake is evaluated by modelling the wake behind a single wind turbine based on the reduced reference flow speed for the turbine. However, changes in ambient turbulence intensity are not considered in the model. The merged wake deficit that arises from the linear superposition of n single turbine wakes is given by

$$\hat{u}(x,y) = 1 - \sum_{i=1}^{n} (1 - \hat{u}_i(x,y)) \tag{9}$$

3.3 | Root sum square superposition

Linear superposition of the velocity deficits of several turbines can result in the non-physical result of negative flow speeds in the combined wake. Katic et al.[38] proposed a model for the superposition of the squares of the velocity deficits, which helps to maintain physically meaningful wake velocities. The cumulative wake deficit is smaller than that predicted for linear superposition. The root-sum-square superposition model assumes that the combined wake deficit at a location is the square root of the quadratic sum of the n upstream single turbine wake deficits.

$$\hat{u}(x,y) = 1 - \sqrt{\sum_{i=1}^{n} \left(1 - \hat{u}_i\,(x,y)\right)^2} \tag{10}$$

4 | SINGLE TURBINE SIMULATIONS

For a single turbine in uniform flow conditions, the integrated power coefficient C_P, thrust coefficient C_T, and tip speed ratio λ are defined as

$$C_P = \frac{P}{\frac{1}{2}\rho A u_\infty^3}, \qquad C_T = \frac{T}{\frac{1}{2}\rho A u_\infty^2}, \qquad \lambda = \frac{\omega d}{2u_\infty} \tag{11}$$

where P and T are the power and thrust of the rotor respectively, ρ is the fluid density, A is the swept area of the turbine rotor, and u_∞ is the freestream hub-height flow speed. Peak C_P is found to be $C_P = 0.53$ for the rotor in the prescribed velocity profile (c.f. $C_P = 0.50$ in uniform flow as defined by Jonkman et al.[14]) due to the flow speed variation across the rotor swept area which affects the mass flow rate through the rotor plane. This is achieved at a slightly higher tip speed ratio than the uniform case, $\lambda = 8.50$ vs. $\lambda = 7.55$. The corresponding turbine thrust coefficient is $C_T = 0.88$. It should be noted that differences in tip loss implementations can affect rotor thrust and power, particularly in non-uniform flows.

Side and frontal contours of streamwise velocity normalised by the freestream hub-height flow speed around a single NREL 5MW reference rotor are shown in Figure 4, where the increase in normalised flow speed with altitude is a consequence of the vertical shear profile. The turbine rotates clockwise, as viewed from the front, and thus anticlockwise angular momentum is induced downstream, resulting in a skewing of the wake with the wake adjacent to the ground moving towards the right as viewed from upstream. The streamwise velocity in the centre of the wake immediately downstream of the rotor is higher than at positions further outboard, as also shown by Martinez-Tossas et al[10]. Two factors contribute to this: blade loading increases with spanwise distance due to the higher relative flow speeds, resulting in greater momentum removal from the

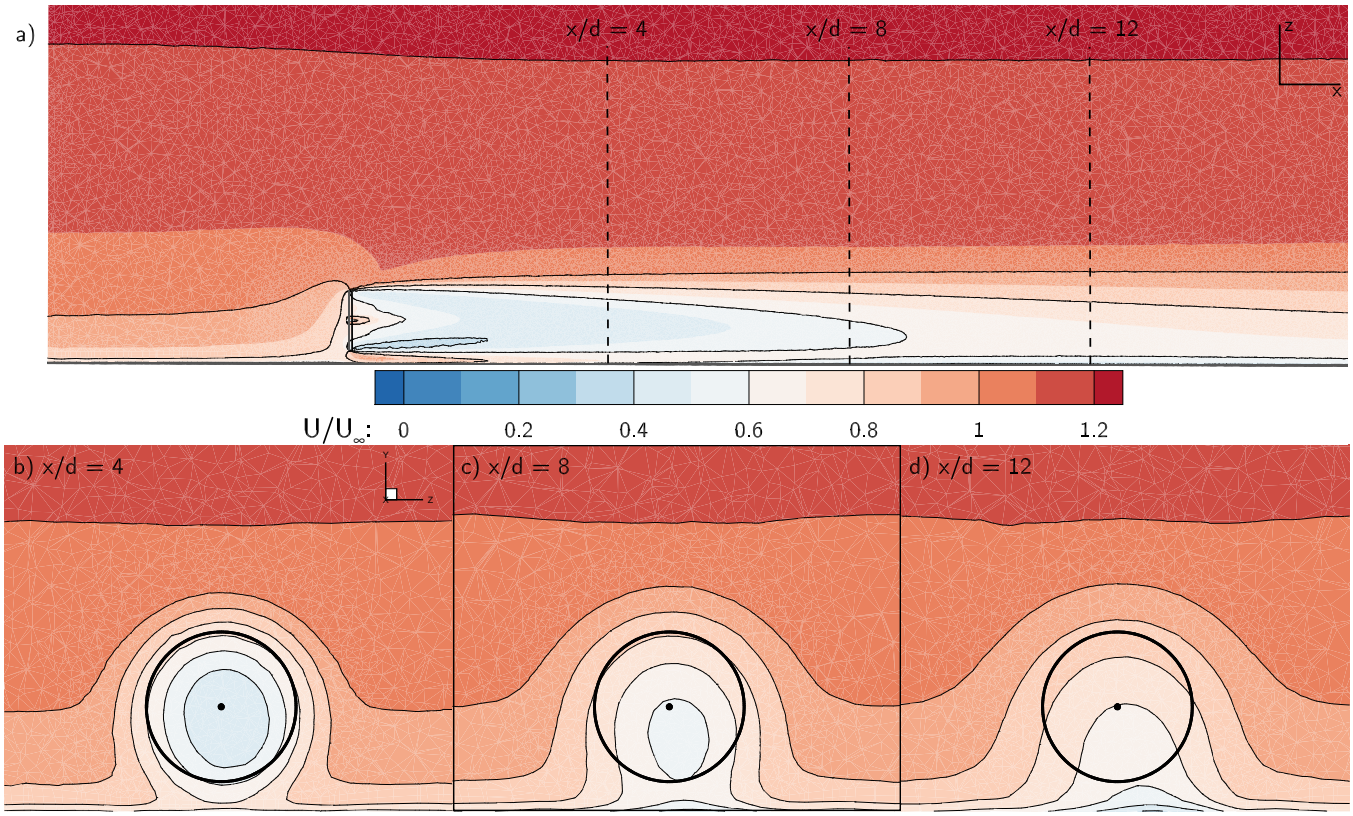

FIGURE 4 Side view (a) and frontal views (b-d) of streamwise velocity normalised by upstream hub-height flow speed for a single turbine operating at peak power coefficient. Frontal views are taken at 4d (b), 8d (c), and 12d (d) downstream of the turbine. The turbine perimeter is marked with a circle.

flow; and the cylindrical root section of the blades impose a relatively small resistance to the flow, resulting in the flow being accelerated around the nacelle. This region of higher flow speeds mixes with the rest of the wake over a distance of approximately two diameters downstream of the rotor. Re-energisation of the wake occurs more quickly from above the wake, as compared to from below, due to greater flow shearing due to higher flow speeds found at higher altitudes in the vertical shear profile. Turbulence intensity is significantly increased in the regions where there is a large difference in flow speed between the wake and ambient flow, resulting in an increased rate of mixing. Consequently, as shown in Figure 4, the wake appears to drop in altitude as it propagates downstream, but this is an artifact of differential rates of wake mixing with respect to the vertical direction due to the velocity profile. Lateral translation of the centre of the wake is also observed due to the swirl imparted on the flow by the BE-AD model.

The effect of ambient turbulent intensity on the recovery of the wake is shown in Figure 5, where the ambient hub-height turbulence intensity is reduced to c. 1% whilst maintaining the same mass flux through the rotor plane as in the higher turbulence intensity case. The reduction in ambient turbulence intensity implies reduced shear in the velocity profile, as shown in Figure 5 (b). In general, the velocity deficit in the wake persists further downstream of the turbine as the rate at which the wake re-energises is reduced. Furthermore, there is reduced asymmetry between the re-energisation of the wake from above and below as the difference in velocity shear above and below, between the wake and ambient flow is

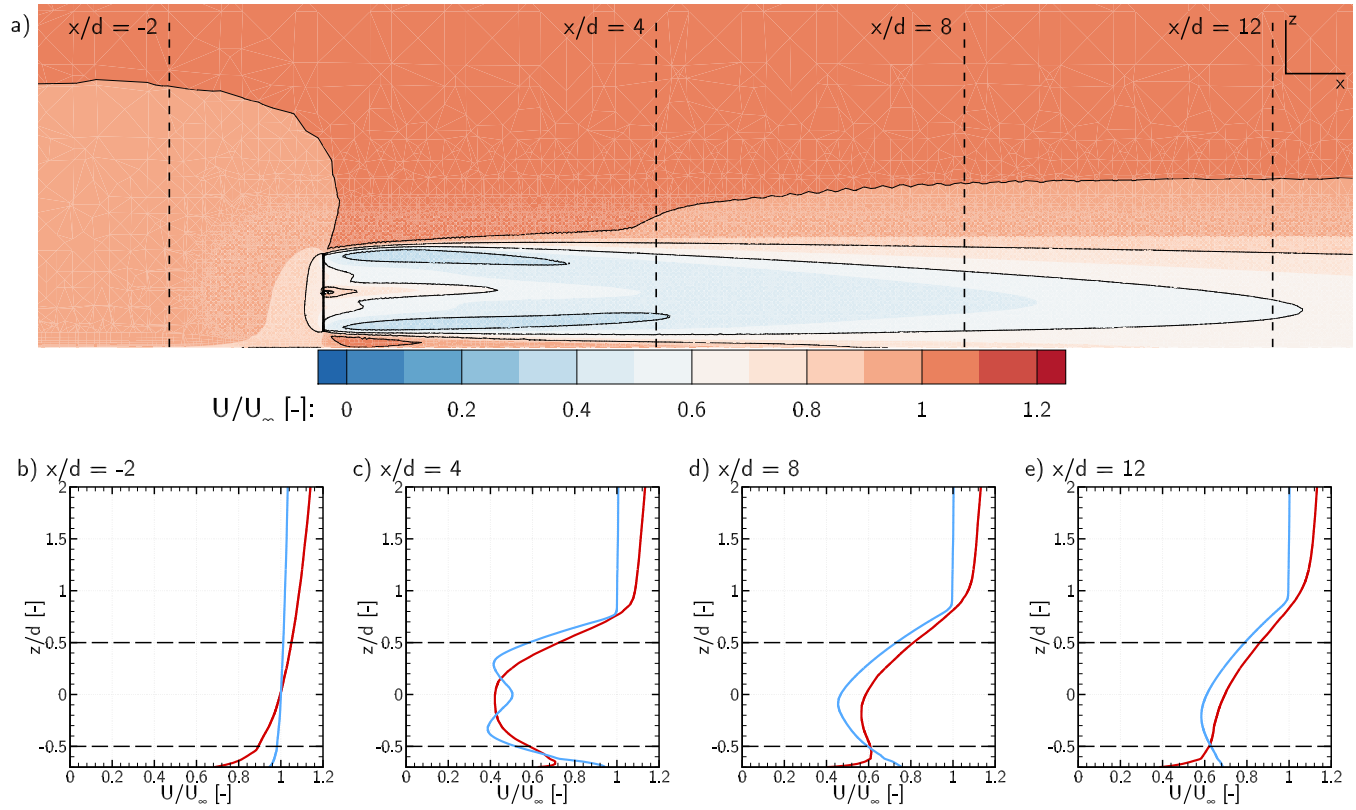

FIGURE 5 Side view (a) of streamwise velocity normalised by upstream hub-height flow speed for a single turbine operating at peak power coefficient in a low ambient turbulence intensity flow. The vertical shear profile is compared between the 1% (blue) and 5.5% (red) turbulence intensity cases in (b-e) upstream and at three locations downstream of the turbine. The vertical position of the rotor is indicated at $z/d = \pm 0.5$ with dashed lines.

reduced. Consequently, while the wake in the lower turbulence intensity flow is more symmetric than previously, the velocity deficit is greater at fixed downstream locations. The wake behind a single turbine in a sheared flow operating at the peak power coefficient is complex and asymmetric.

5 | MULTI-TURBINE SIMULATIONS

Deploying a second wind turbine 8d downstream of, and inline with, the first turbine has very little impact on the power and thrust of the upstream turbine, as shown in Table 2, where it should be noted that the C_P, C_T, and λ values are referenced to the flow speed 2.5d upstream of the respective turbine. However, as noted elsewhere in experimental and numerical studies [1,5], there is a significant decrement in performance for the second turbine, operating in waked conditions. Whilst the reference flow speed for the downstream turbine in the inline configuration is 6.01ms^{-1}, the spatial average of the flow speed approaching the turbine is $\langle U \rangle = 6.41\text{ms}^{-1}$ due to the recovery of flow speed at larger radii. The magnitude of the momentum and kinetic fluxes approaching the turbine are also affected by the wake, with $\langle U^2 \rangle^{1/2} = 6.48\text{ms}^{-1}$ and $\langle U^3 \rangle^{1/3} = 6.55\text{ms}^{-1}$ respectively. This can be beneficial for thrust and power coefficients as the fluxes through the rotor are higher than implied by a single upstream flow speed measurement. For the inline configuration, the second turbine operates at 28.4% of the power and 42.4% of the thrust of the upstream

TABLE 2 Turbine power C_P and thrust C_T coefficients and tip speed ratio λ for below-rated flow speed conditions, $u_\infty = 9.0\ ms^{-1}$, for the single turbine and three wake combination cases. Note that the reference flow speed is defined as the hub-height centreline flow speed 2.5d upstream of the respective turbine.

	Single	Inline		Offset y = 1d		Offset y = 1.75d	
Turbine		Upstream	Downstream	Upstream	Downstream	Upstream	Downstream
Reference U [ms^{-1}]	9.0	9.0	6.01	9.0	8.49	9.0	8.98
C_P	0.53	0.52	0.50	0.52	0.49	0.52	0.53
C_T	0.88	0.88	0.84	0.88	0.95	0.88	0.90
λ	8.50	8.48	8.35	8.48	8.78	8.48	8.55
P [MW]	2.95	2.90	0.83	2.90	2.29	2.90	2.93
T [MN]	0.54	0.54	0.23	0.54	0.52	0.54	0.55

turbine. As shown in Figure 6, the first turbine's wake reduces the energy available to the second turbine, although the combined wake recovers faster downstream of the second turbine as the wake diffuses into a flow with higher ambient turbulence (due to being encompassed by the first wake). Consequently, a third turbine 8d downstream from, and inline with, the second turbine would extract slightly higher power than the second turbine, a qualitative result that has been seen in, for example, the Lillgrund wind farm[39]. For inline turbines, at $x/d = 16$, hub-height $U/U_\infty = 0.598$ with two upstream turbines, compared to at $x/d = 8$ $U/U_\infty = 0.585$ with one upstream turbine.

Variations in the flow incident upon the second turbine ($x = 8d$ downstream from the first turbine) and at the location of a hypothetical third turbine at $x = 16d$ are shown in Figure 7. Variations in the flow incident upon the downstream rotor lead to the variations in turbine performance noted above, which in turn affect how the combined wake propagates downstream. Shifting the downstream turbine laterally by $y = 1d$, so that the rotor nacelle is aligned with the $U = 0.99U_\infty$ boundary of the wake from the upstream turbine means that there is a much flux of mass, momentum and kinetic energy through the second turbine than in the inline case. The spatially-averaged flow speed approaching the downstream turbine $\langle U \rangle = 8.33 ms^{-1}$, whereas $\langle U^2 \rangle^{1/2} = 8.83 ms^{-1}$ and $\langle U^3 \rangle^{1/3} = 9.16 ms^{-1}$ respectively. Note that higher powers of $\langle U \rangle$ may be greater than the free stream hub height flow speed due to the vertical shear profile. Consequently, the power achieved by the second turbine increases substantially, to 94.2% of the first turbine. Turbine thrust is 8% higher than the upstream turbine. Shifting the downstream laterally by $y = 1.75d$ from the centreline results in the second turbine being fully out of the wake of the upstream turbine, and thus the differences in turbine performance and approaching fluxes are negligible (see Table 1).

Flow speed variation across the second rotor's plane at $x = 8d$ has two origins; the vertical shear profile, and the impact of the upstream wake. In Figure 7 (d) this variation is due to the vertical shear profile as the turbine is outside the wake of the upstream device. However, particularly in (c), there is azimuthal asymmetry in the flow due to the presence of the upstream wake. The impact of the upstream wake on the downstream turbine is more significant closer to the axis of the upstream turbine. The variation in flow conditions (both lateral and vertical shear) near the rotor blade tips poses challenges for tip loss modelling in actuator disk and line methods, as such models usually assume that the ambient flow around the turbine is uniform[40,41].

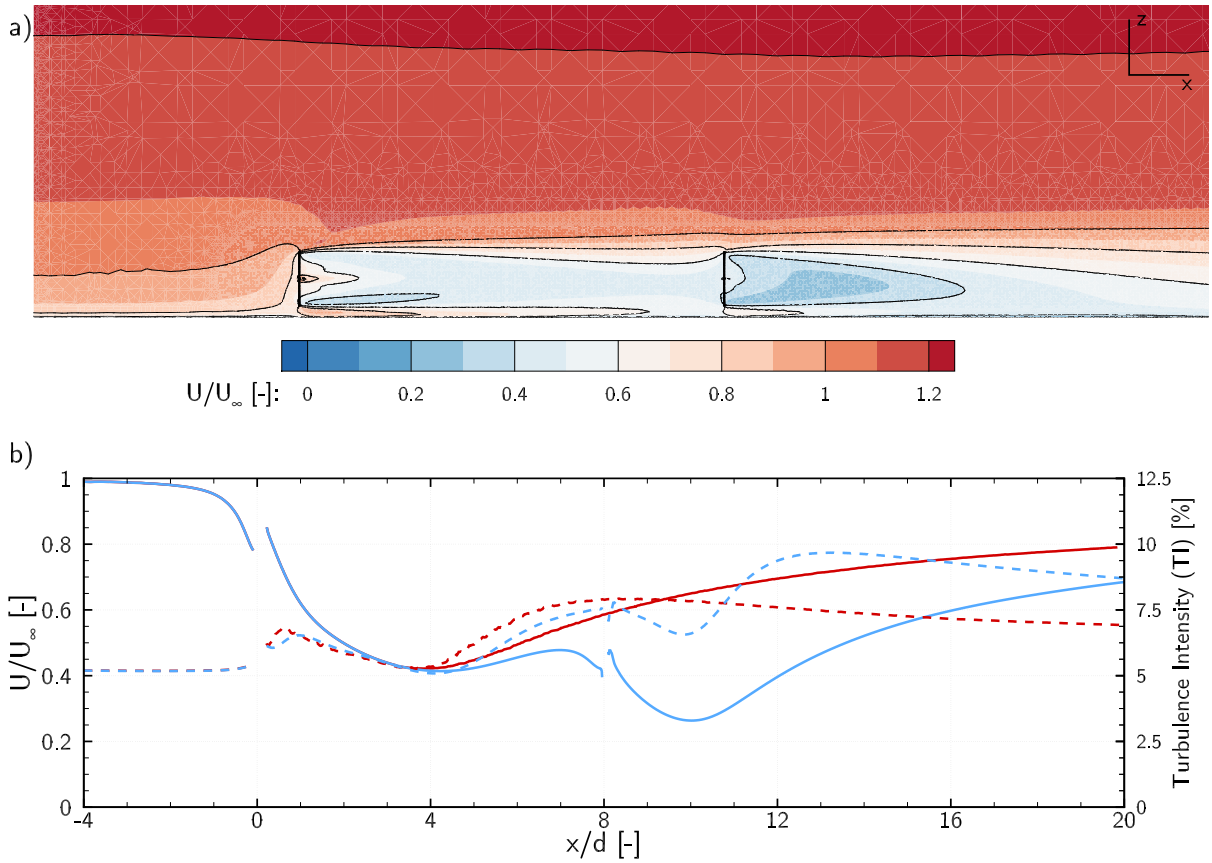

FIGURE 6 Side view (a) and streamwise hub-height centreline variation in axial flow speed (solid) and turbulence intensity (b) past two identical rotors operating at peak power coefficient. The turbines are located at $x/d = 0$ and $x/d = 8$. The streamwise variation in hub-height axial flow speed and turbulence intensity for a single turbine are also shown in (b) (red). Flow velocities are normalised on the hub-height free stream velocity 2.5d upstream of the first turbine.

Plots (e) to (h) in Figure 7 show the streamwise velocity contours of the combined wakes at $x = 16d$, the location of a hypothetical third turbine. For the inline case (f), the velocity deficit is increased, but otherwise similar in structure to that behind a single turbine (a) and (e) at different distances, as the second turbine reduces the momentum in the wake along the same axis as the first turbine. The laterally offset case (g) and (h) exhibit the development of an emergent structure from the combined wakes, as there is spatial variation in the momentum deficit and turbulence intensity within the wake region. This introduces additional complexity for wake superposition models, as discussed in Section 6. For the laterally fully offset case the wake at $x = 16d$ approximates the superposition of wakes at 8d and 16d behind the single rotor, consistent with the relatively unperturbed performance of the fully laterally offset turbine (Table 1).

5.1 | Above rated flow speed operation

Rated power control of the NREL 5MW reference turbine is provided by pitching the blades to feather and changing the turbine tip speed ratio (holding ω constant), thereby reducing the rotor thrust forces which results in a smaller velocity deficit in the wake, as shown in Figure 8. The momentum removed from the flow represents an increasingly small fraction of the available kinetic flux as the flow speed increases, and hence the

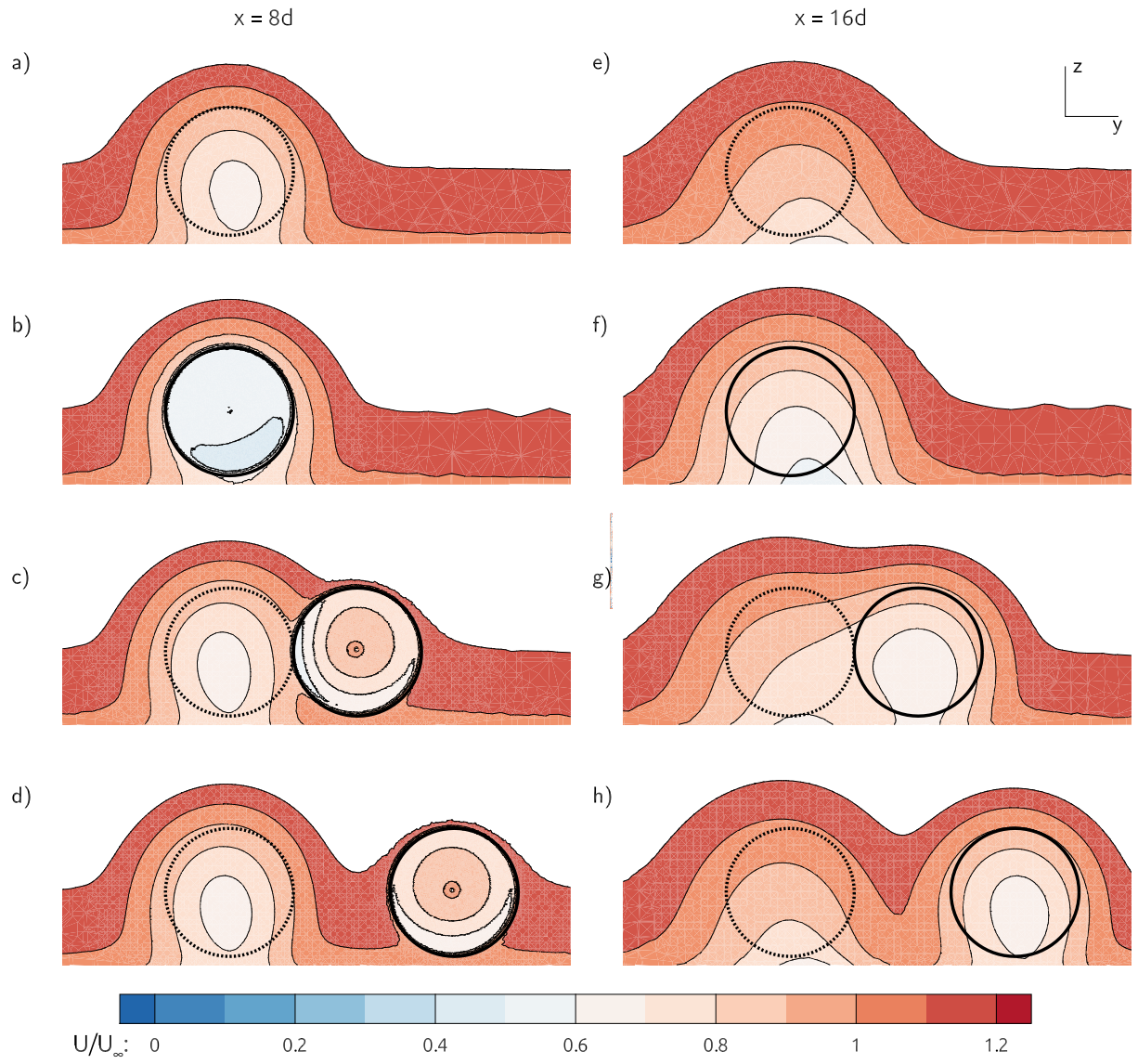

FIGURE 7 Frontal (y-z plane) view of streamwise velocity contours at $x = 8d$ (at the location of the second turbine) (a-d), and $x = 16d$ downstream of the first turbine (e-h). The evolution of the flow profile is shown in (a) and (e) for the single turbine, (b) and (f) for the inline turbines, (c) and (g) with the downstream turbine laterally offset by 1d, and (d) and (h) for the downstream turbine laterally offset by 1.75d. The hub-height inlet flow speed is $u_\infty = 9.0$ ms^{-1}. The projected location of the upstream turbine is indicated with a dashed circle, and a solid circle for the downstream turbine.

wake deficit relative to the freestream flow becomes smaller. However, the reducing flow speed difference between the wake and ambient flows means that less turbulence is generated in the shear region between the two flows, reducing the rate at which the mixing processes drive wake recovery. There is therefore a non-linear interaction above rated flow speed in the recovery of the wake velocity through the reduced momentum removal from the flow and the reducing level of turbulence induced from shear between the ambient and wake flows. On balance, the wake recovers over shorter streamwise distances at higher freestream flow speeds. For the single turbine case and maintaining turbulence intensity at 5.5%, it was found that the streamwise distance for the centreline hub-height flow speed to recover to the through-rotor flow speed reduced from approximately 20d below rated flow speed (at $u_\infty = 9.0$ ms^{-1}), to approximately 4d at $u_\infty = 14.0$ ms^{-1}, and 1.5d at $u_\infty = 18.0$ ms^{-1}.

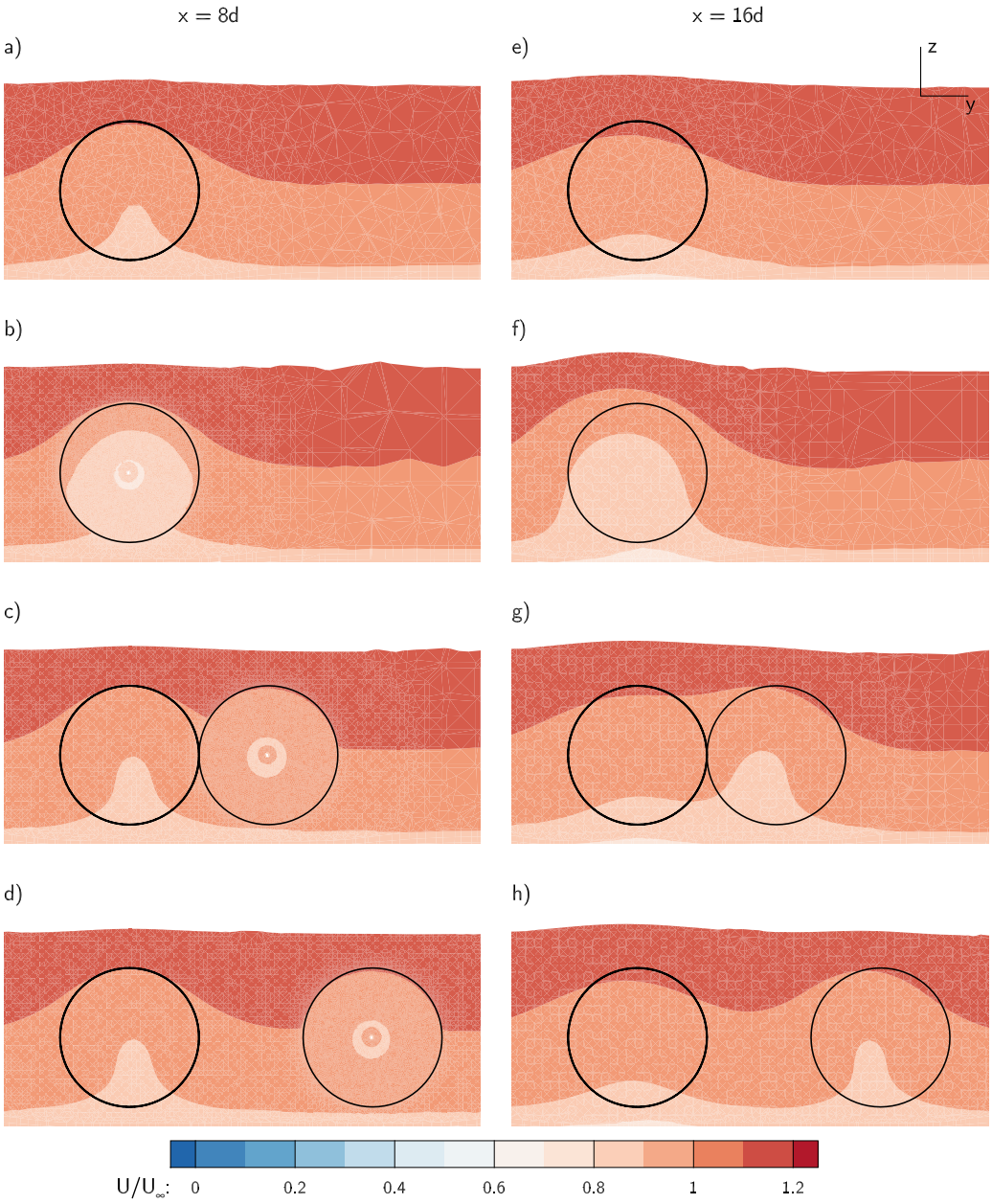

FIGURE 8 Frontal (y-z plane) view of streamwise velocity at $x = 8d$ (at the location of second turbine) (a-d), and $x = 16d$ downstream of the first turbine (e-h). The evolution of the flow profile is shown in (a) and (e) for the single turbine, (b) and (f) for the inline turbines, (c) and (g) with the downstream turbine laterally offset by 1d, and (d) and (h) for the downstream turbine offset by 1.75d. The hub-height inlet flow speed is $u_\infty = 16.0\ \mathrm{ms}^{-1}$. The projected location of the upstream turbine is indicated with a dashed circle, and a solid circle for the downstream turbine.

Frontal (y-z) plane contours of streamwise flow speed at the $x = 8d$ and $x = 16d$ downstream of the first turbine, are shown in Figure 8, presented for the case where the hub-height freestream flow speed is $u_\infty = 16.0\ \mathrm{ms}^{-1}$. It can be seen through comparison to Figure 7 that the velocity deficit is smaller when operating above rated flow speed, although there is still slower re-energisation of the wake at lower altitudes. The downstream turbine in the inline case operates in the wake and is hence affected by the operation of the upstream turbine, whereas the two

TABLE 3 Turbine power C_P and thrust C_T coefficients and tip speed ratio λ for above rated flow speed conditions, $u_\infty = 16.0\,\mathrm{ms}^{-1}$, for the single turbine and three wake combination cases. Note that the reference flow speed is defined as the hub-height centreline flow speed 2.5d upstream of the respective turbine, and that all turbines produce 5 MW above rated flow speed.

	Single	Inline		Offset $y = 1d$		Offset $y = 1.75d$	
Turbine		Upstream	Downstream	Upstream	Downstream	Upstream	Downstream
Reference U [ms^{-1}]	16.0	16.0	14.3	16.0	15.4	16.0	15.9
C_P	0.16	0.16	0.28	0.16	0.18	0.16	0.16
C_T	0.20	0.20	0.31	0.20	0.21	0.20	0.20
λ	6.48	6.48	7.78	6.48	6.60	6.48	6.52

laterally offset turbines are largely unaffected by the wake of the upstream turbine. The hub-height reference flow speed for the downstream turbine in the inline case is approximately $u = 14.3\,\mathrm{ms}^{-1}$, and although the blades of the second turbine are also pitched-to-feather, the turbine thrust is higher than that behind the first turbine, as detailed in Table 3. Consequently, the wake deficit is larger behind the second turbine than the first, in contrast to the case when the upstream turbine was at rated flow speed. As in the rated flow speed case, the combined wake at $x = 16d$ is similar in spatial structure to the single turbine case for rated power operation, albeit with a larger velocity deficit due to the second turbine.

In contrast to the earlier rated flow speed simulations, the second turbine laterally offset by 1d from the upstream turbine now operates almost entirely outside of the wake of the first turbine which has largely recovered, and hence the azimuthal flow asymmetry across the rotor plane is significantly reduced from the previous case. The difference in thrust between the two turbines is less than 0.5%. However, the combined wake at $x = 16d$ exhibits the same emergent multi-turbine wake structure, with re-energisation of the wake occurring at a lower rate in the region where the wakes merge. The rotor laterally offset by 1.75d is unaffected by the presence of the upstream turbine, and hence there is no appreciable difference in turbine thrust or power. Furthermore, there is little interaction between the wakes downstream of the two turbines at $x = 16d$ downstream from the first turbine ($x = 8d$ from the second).

6 | SUPERPOSITION MODELS

Three widely used superposition models, largest deficit superposition, linear superposition, and root-sum-square superposition are compared the wakes observed in the CFD simulations for each of the spatial and operational cases described previously. All three superposition models consider the superposition of single, independent wakes, which are derived from the RANS BE AD simulations of a single turbine to ensure consistency with the multi-rotor CFD simulations against which the combined wake predictions are compared.

Two features of the combined wakes are compared to evaluate the performance of the wake superposition models: the largest relative discrepancy between the models and the simulation data; and the cumulative difference between the models and the simulation data. These metrics are described in terms of the simulated velocity deficit, $f_s(y/d) = 1 - u(y/d)/u_\infty$, and the deficit determined by the superposition model, $f_m(y/d)$.

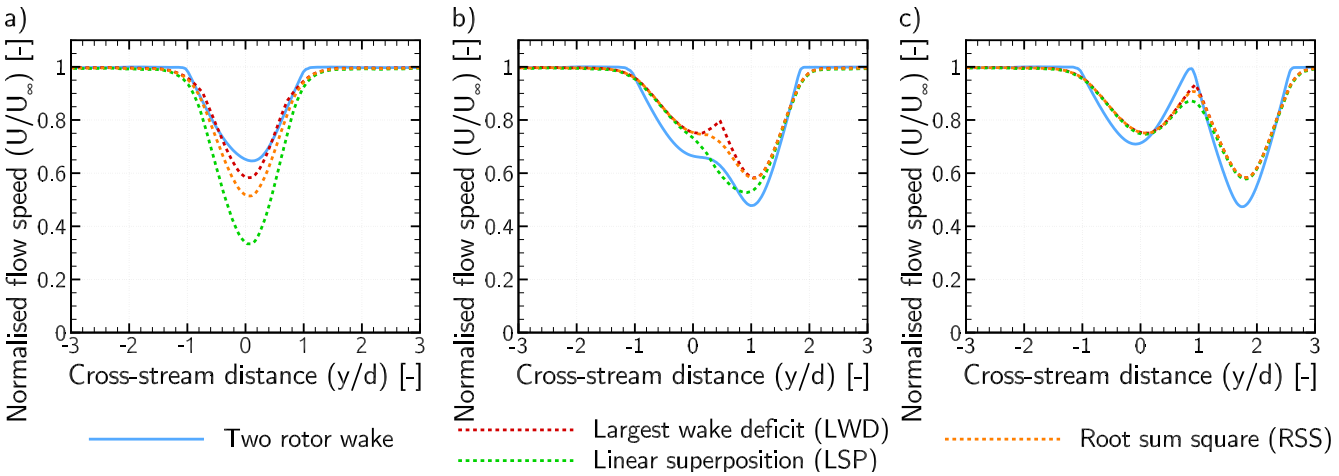

FIGURE 9 Cross-stream variation in normalised streamwise flow speed u/u_∞ for the three multi-rotor cases at $x = 16d$ downstream from the first rotor. The freestream hub-height flow speed upstream of the first turbine is $u_\infty = 9.0 ms^{-1}$. Computational results from the RANS simulations are indicated with a solid line, and the three superposition models are shown with dashed lines. The inline case is shown in (a), (b) shows the 1d lateral offset case, and (c) shows the 1.75d lateral spacing case. The cross-stream distance is measured relative to the upstream turbine.

Although velocity deficits are spatially varying everywhere, we consider here just their lateral variation, i.e. as a function of y/d. The relative discrepancy is defined as the residual, $\hat{r}$, between the model and data, normalised relative to $f_s(y/d)$ in order to penalise discrepancies between the two when the velocity deficit is large (i.e., low flow speeds and high thrust operation):

$$\hat{r} = \left| \frac{f_m(y/d) - f_s(y/d)}{f_s(y/d)} \right|. \tag{12}$$

The cumulative difference, ϵ^2, between the two curves is also normalised with respect to $f_s(y/d)$, and describes the overall magnitude of the differences between the predictions of the superposition models and the simulated data:

$$\epsilon^2 = \int_{-\infty}^{\infty} \left(\frac{f_m(y/d) - f_s(y/d)}{f_s(y/d)} \right)^2 d(y/d). \tag{13}$$

6.1 | Below rated flow speed

Figure 9 compares the normalised streamwise velocity from the RANS simulations to that predicted by the wake superposition models for the three multi-rotor cases at the location of a hypothetical third turbine, $x = 16d$ downstream from the first rotor when the freestream hub-height flow speed is $u_\infty = 9.0 ms^{-1}$, within the power maximisation control region. This represents a condition where the impact of energy extraction on the flow is maximised.

All the superposition methods predict that the maximum velocity deficit occurs in the correct spatial location for the inline turbine configuration. However, whereas the the largest wake deficit (LWD) model predicts fairly well the simulated velocity profile ($\hat{r}_{max} = 0.1036$, $\epsilon^2 = 0.0052$), the linear superposition (LSP) model significantly over-predicts the velocity deficit ($\hat{r}_{max} = 0.4854$, $\epsilon^2 = 0.1663$), as shown in Table 4. The LSP and, to a lesser extent, the root-sum-square (RSS) superposition models perform worse than the LWD model because the CFD simulated wake recovers

TABLE 4 Maximum deviation $\hat{r}_{max}$ and error ϵ^2 metrics for three wake combination cases using the largest wake deficit (LWD), linear superposition (LSP) and root sum square (RSS) superposition models when the hub-height freestream flow speed is below rated ($u_\infty = 9.0$ ms^{-1}).

	Inline		Offset y = 1d		Offset y = 1.75d	
	$\hat{r}_{max}$	ϵ^2	$\hat{r}_{max}$	ϵ^2	$\hat{r}_{max}$	ϵ^2
LWD	0.1036	0.0052	0.2696	0.0642	0.2419	0.0348
LSP	0.4854	0.1663	0.1236	0.0172	0.2309	0.0335
RSS	0.2082	0.0257	0.2191	0.0474	0.2418	0.0351

more quickly behind the second turbine than in the single turbine case used to parameterise the superposition models. The superposition models do not accurately predict wake width, which depends on the enhanced rate of mixing due to increased turbulence levels as the second wake expands into the upstream turbine wake.

As discussed in Section 5, the combined wake that develops in cases where the downstream turbine is laterally offset results in a wake that is a function of the lateral spacing between the turbines and the thrust of the potentially partially waked downstream turbine. The rate at which the wake is re-energised is reduced in the region where the two wakes impinge upon each other due to the reduced availability of high momentum ambient flow, although the turbulence intensity may be increased. This may occur even when the downstream turbine is not itself in the wake of the upstream turbine. Consequently, in the case of a partially offset wake, $y/d = 1$, the LWD model, which does not model any interactions between the wakes has the worst wake predictions $\hat{r}_{max} = 0.2696$ and $\epsilon^2 = 0.0642$, in contrast to the inline case where it was the best performing model. The LWD model underpredicts the wake deficit across large portions of the wake, predicting in particular that the wake deficit reduces between the two rotors. The LSP model, worst in the inline case, performs best of the three models ($\hat{r}_{max} = 0.1236$, $\epsilon^2 = 0.0172$), although this agreement is not as good as the LWD model for the inline case. However, the u/u_∞ profile predicted by the RSS superposition model most closely represents the shape of the simulated wake profile, although the wake deficit is underpredicted, worsening $\hat{r}_{max}$ and ϵ^2 for the model.

Increasing the lateral spacing between the turbines to 1.75d, so that the second turbine operates outside the wake of the first, means that similar levels of momentum are removed from the flow by the two turbines. As in the previous case, the second turbine wakes propagate into a region with reduced kinetic flux and different levels of turbulence intensity from the single turbine case, affecting the development of the combined wake. All three wake superposition models predict similar wake profiles, and consequently both $\hat{r}_{max} \approx 0.24$ and $\epsilon^2 \approx 0.0345$ metrics are similar for all the models. The increased turbulence intensities in the wake regions of the turbines drive different rates of wake recovery that the superposition models of two wakes are unable to represent and they consequently uniformly underestimate the maximum velocity deficit behind both turbines, and overestimate the velocity deficit between the two turbines at 16d downstream.

Incorrectly predicting the velocity deficit can lead to significant errors in the predicted thrust and power. CFD simulation of a third turbine equally spaced and inline with the inline turbine case resulted in a power of 0.93 MW and a thrust of 0.28 MN, slightly greater than that for the second turbine. However, this increase in thrust and power is not predicted with the superposition models, with LWD superposition predicting 0.64 MW, RSS predicting 0.48 MW, and LSP substantially underestimating power at 0.12 MW. The superposition methods also underestimate

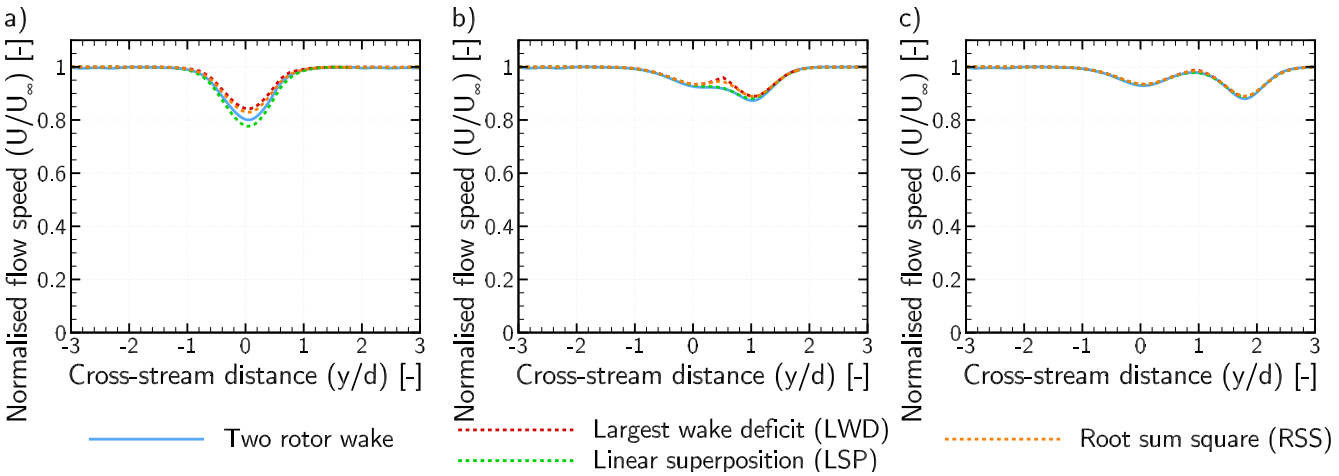

FIGURE 10 Cross-stream variation in normalised streamwise flow speed u/u_∞ for the three multi-rotor cases at $x = 16d$ downstream from the first rotor. The freestream hub-height flow speed upstream of the first turbine is $u_\infty = 16.0 ms^{-1}$. Computational results from the RANS simulations are indicated with a solid line, and the three superposition models are shown with dashed lines. The inline case is shown in (a), (b) shows the 1d lateral offset case, and (c) shows the 1.75d lateral spacing case. The cross-stream distance is measured relative to the upstream turbine

the thrust on the third turbine. When the third turbine is centred $z = 1d$ offset from the first (inline) two, the power predicted via simulation is 2.36 MW. LWD superposition achieved close agreement of 2.14 MW, however the RSS and LSP methods substantially underestimated power at 1.56 MW and 0.84 MW respectively. In all cases thrust was underestimated using the superposition methods, although the LWD method when the third turbine was laterally offset by $z = 1d$ achieved agreement within 10% of the simulated value. Underestimation of the thrust may have adverse implications for prediction of turbine loading. However, in some cases, such as when the second turbine is $z = 1d$ laterally offset from the first, the superposition methods overpredicted the flow speeds approaching a third turbine. This results in overestimation of thrust and power of the third turbine.

6.2 | Above rated flow speed operation

When the freestream flow speed is above $u_r = 11.4 ms^{-1}$ for the NREL 5MW reference turbine, the turbine blades are pitched to feather in order to reduce rotor torque. The momentum removed from the flow is reduced, and the velocity deficit in the wake recovers over a shorter streamwise distance, as discussed in Section 5.1. As shown in Figure 10, and summarised in Table 5, this affects how well the wake superposition methods predict the combined wake at $x = 16d$.

Both turbines operate above rated flow speed when the turbines are inline and the freestream hub-height flow speed is $u_\infty = 16.0 ms^{-1}$. The downstream turbine experiences a lower flow speed than the first due to the presence of the wake, and hence the blade root pitch feather angle is smaller (8.8° vs. 10.3°). Consequently, the thrust of the downstream turbine is higher than that of the upstream turbine, contrary to the rated flow speed case, affecting the development of the combined wake. The LWD superposition model which performed best in the rated flow speed case, has the worst $\hat{r}_{max}$ and ϵ^2 metrics in the rated power case. Instead, the LSP model, which performed worst in the rated flow speed case, now has the smallest maximum difference between the superposition model and simulated flow data, $\hat{r}_{max} = 0.0303$, and the closest overall agreement with

TABLE 5 Maximum deviation $\hat{r}_{max}$ and error ϵ^2 metrics for three wake combination cases using the largest wake deficit (LWD), linear superposition (LSP) and root sum square (RSS) superposition models when the hub-height freestream flow speed ($u_\infty = 16.0 ms^{-1}$) is above the rated flow speed.

	Inline		Offset $y = 1d$		Offset $y = 1.75d$	
	$\hat{r}_{max}$	ϵ^2	$\hat{r}_{max}$	ϵ^2	$\hat{r}_{max}$	ϵ^2
LWD	0.0526	0.0020	0.0452	0.0008	0.0108	0.0001
LSP	0.0303	0.0007	0.0098	0.0001	0.0092	0.0001
RSS	0.0361	0.0009	0.0276	0.0005	0.0106	0.0001

the simulated flow profile, $\epsilon^2 = 0.0007$. The LSP model still overestimates the maximum velocity deficit, whereas the RSS model underestimates the deficit, with only marginally worse agreement with the simulated wake data, $\hat{r}_{max} = 0.0361$ and $\epsilon^2 = 0.0009$. The underestimation by the RSS model arises from the velocity deficit of the upstream wake at $x = 16d$ being small compared to the wake from the second turbine.

The reduction in thrust, and therefore the reduced velocity deficit, that occurs when operating above the rated flow speed means that the laterally offset downstream turbines are less affected by the upstream wake and consequently turbine thrust and power is very similar to that of the upstream turbine. In the lateral separation $y = 1d$ case, Figure 10 shows that the LWD model does not predict the combined wake the develops between the two models, and hence has the poorest agreement with the simulated data as measured by the $\hat{r}_{max}$ and ϵ^2 metrics. The LSP model agrees well with the simulated data ($\hat{r}_{max} = 0.0098$, $\epsilon^2 = 0.0001$), suggesting that, for the small thrusts observed above rated flow speed, the combination of the velocity deficits is to a first approximation a linear process. The RSS model performs better than the LWD model, but not as well as linear superposition. When the lateral separation is increased further to $y = 1.75d$, the interactions between the turbines reduce further, and there is little difference between the $\hat{r}_{max}$ and ϵ^2 metrics of the three wake superposition models, although the LSP model again performs best overall.

7 | DISCUSSION & CONCLUSIONS

Wake interaction and evolution depends on the spatial configuration and the operating regime of the turbines. When the freestream hub-height flow speed was below the rated flow speed, the thrust of the upstream turbine was maximised, resulting in the largest velocity deficit in the wake. This reduced the power available to the second turbine in the inline case, concurring with the findings of other studies [5]. The elevated turbulence intensity level means that the velocity deficit in the wake of the second turbine recovers more quickly than after the first turbine, and consequently at the position of a hypothetical third turbine at $x = 16d$, a higher incident flow speed, and hence higher power, would be experienced than by the second. This result has also been observed in offshore wind farms [1]. The thrust of the first turbine reduces as the blades pitch to feather above rated flow speed, reducing the velocity deficit in the wake. The turbulence intensity in the wake of the first turbine is reduced due to the reduced shear between the wake and ambient flow, and thus the rate at which the wake re-energises is reduced. When both turbines operate above the rated flow speed, the thrust of the second turbine is necessarily greater than the first, resulting in a larger wake deficit than the first turbine which

then persists further downstream of the second turbine, which may impact upon the operation and subsequent wake interactions of additional turbines in the wind farm.

In wake modelling it is often assumed that the turbine wake is axisymmetric. Azimuthal variation in incident flow speed, and hence thrust and power, was observed when the downstream turbine was laterally offset from the upstream device such that only part of the rotor swept area lay within the upstream turbine wake. In the lateral offset case, this resulted in asymmetric re-energisation of the upstream wake and the formation of a complex combined wake. In offset conditions below rated flow speed, the impact of the second turbine's wake on the first turbine's wake was observed even when the second turbine itself was unaffected by the upstream turbine. In offset conditions above rated flow speed the incident flow speed, $u_\infty = 16.0\ ms^{-1}$, for all the turbines was almost the same due to smaller wakes, such that the turbine thrust and power were similar. However, the wake combination and evolution was still affected by the lateral spacing between the turbines through the interactions of the wakes.

Three common wake superposition models were compared to RANS-CFD simulation in this study: largest wake deficit (LWD) superposition, linear superposition (LSP), and root-sum-squared (RSS) superposition. The superposition models are parameterised in terms of the hub-height wake behind a single turbine, simulated in RANS CFD, and were evaluated at the location of a hypothetical turbine $x = 8d$ downstream from the second turbine. LWD superposition was the best performing model for the inline case below rated flow speed, although it was found that this was the worst performing model in the lateral offset $y = 1d$ case. In contrast, LSP was the worst performing model for the inline case at rated flow speed and was the best performing model in the lateral offset $y = 1d$ case, although the shape of the wake profile was better predicted by the RSS model. All three superposition models predicted very similar velocity deficit profiles in the lateral offset $y = 1.75d$ case, although the error metrics were larger than the best performing models for the other turbine configurations. Above rated flow speed, it was found that the LSP model provided the best agreement with the RANS CFD data for all interaction cases, although there was little difference between the models in the lateral offset $y = 1.75d$ case due to smaller wake deficits and large spatial separation. Consequently, the best choice of existing wake superposition models for predicting the combined wake depends on both how the turbines are operating and the layout of the turbines. Further work will be required to better understand the impact of ambient flow conditions and azimuthal asymmetry on turbine performance and subsequent wake development in order to inform the development of improved wake models.

ACKNOWLEDGMENTS

The authors would like to acknowledge the support of the Oxford Advanced Research Computing facility and E.ON Climate and Renewables (UK).

References

1. Barthelmie R. J., Hansen K. S., Frandsen S. T., et al. Modelling and Measuring Flow and Wind Turbine Wakes in Large Wind Farms Offshore. *Wind Energy.* 2009;12:431-444.

2. Sanderse B.. *Aerodynamics of Wind Turbine Wakes Literature Review.* Technical Report ECN-E-09-016: Energy Research Centre of the NetherlandsPetten, Netherlands; 2009.

3. Göçmen T., van der Laan P., Réthoré P.-E., Pena Diaz A., Larsen G. C., Ott S.. Wind Turbine Wake Models Developed at the Technical University of Denmark: A Review. *Renewable and Sustainable Energy Reviews.* 2016;60:752-769.

4. Vermeer L. J., Sørensen J. N., Crespo A.. Wind Turbine Wake Aerodynamics. *Aerospace Sciences.* 2003;39:467-510.

5. Adaramola M. S., Krogstad P.-Å.. Experimental Investigation of Wake Effects on Wind Turbine Performance. *Renewable Energy.* 2011;36:2078-2086.

6. Tian L. L., Zhu W. J., Shen W. Z., Sørensen J. N., Zhao N.. Investigation of Modified AD/RANS Models for Wind Turbine Wake Prediction in Large Wind Farm. *Journal of Physics: Conference Series.* 2014;524:012151.

7. van der Laan P., Sørensen N. N., Réthoré P.-E., et al. An Improved k Model Applied to a Wind Turbine Wake in Atmospheric Turbulence. *Wind Energy.* 2015;18(5):889-907.

8. Forsting A. R. M., Troldborg N., Gaunaa M.. The Flow Upstream of a Row of Aligned Wind Turbine Rotors and Its Effect on Power Production. *Wind Energy.* 2017;20:63-77.

9. Storey R. C., Norris S. E., Stol K. A., Cater J. E.. Large Eddy Simulation of Dynamically Controlled Wind Turbines in an Offshore Environment. *Wind Energy.* 2013;16:845-864.

10. Martinez-Tossas L. A., Churchfield M. J., Leonardi S.. Large Eddy Simulations of the Flow Past Wind Turbines: Actuator Line and Disk Modeling. *Wind Energy.* 2015;18:1047-1060.

11. Stevens R. J. A. M., Gayme D. F., Meneveau C.. Effects of Turbine Spacing on the Power Output of Extended Wind Farms. *Wind Energy.* 2016;19:359-370.

12. Machefaux E., Larsen G. C., Murcia Leon J. P.. Engineering Models for Merging Wakes in Wind Farm Optimization Applications. *Journal of Physics: Conference Series.* 2015;625:012037.

13. Gunn K., Stock-Williams C., Burke M., et al. Limitations to the Validity of Single Wake Superposition in Wind Farm Yield Assessment. *Journal of Physics: Conference Series.* 2016;749:012003.

14. Jonkman J., Butterfield S., Musial W., Scott G.. *Definition of a 5-MW Reference Wind Turbine for Offshore System Development.* Technical Report NREL/TP-500-38060: National Renewable Energy LaboratoryGolden, Colorado; 2009.

15. Hansen M. O. L, Sørensen J. N., Voutsinas S., Sørensen N. N., Madsen H. Aa.. State of the Art in Wind Turbine Aerodynamics and Aeroelasticity. *Progress in Aerospace Sciences.* 2006;42:285-330.

16. Burton T., Jenkins N., Sharpe D. J., Bossanyi E. A.. *Wind Energy Handbook*. West Sussex, UK: John Wiley & Sons Ltd.; 2011.

17. McIntosh S. C., Fleming C. F., Willden R. H. J.. Embedded RANS-BEM Tidal Turbine Design. In: :10; 2011; Southampton, UK.

18. Réthoré P.-E., van der Laan P., Troldborg N., Zahle F., Sørensen N. N.. Verification and Validation of an Actuator Disc Model. *Wind Energy*. 2014;17(6):919-937.

19. Troldborg N., Zahle F., Réthoré P.-E., Sørensen N. N.. Comparison of Wind Turbine Wake Properties in Non-Sheared Inflow Predicted by Different Computational Fluid Dynamics Rotor Models. *Wind Energy*. 2015;18(7):1239-1250.

20. Shives M., Crawford C.. Adapted Two-Equation Turbulence Closures for Actuator Disk RANS Simulations of Wind & Tidal Turbine Wakes. *Renewable Energy*. 2016;92:273-292.

21. Hennen J., Kenjereš S.. Contribution to Improved Eddy-Viscosity Modeling of the Wind Turbine - to - Wake Interactions. *International Journal of Heat and Fluid Flow*. 2017;68:319-336.

22. Vogel C. R., Willden R. H. J.. Multi-Rotor Tidal Stream Turbine Fence Performance and Operation. *International Journal of Marine Energy*. 2017;19:198-206.

23. Pierella F., Krogstad P.-Å., Sætran L.. Blind Test 2 Calculations for Two In-Line Model Wind Turbines Where the Downstream Turbine Operates at Various Rotational Speeds. *Renewable Energy*. 2014;70:62-77.

24. Sanderse B., van der Pijl S. P., Koren B.. Review of Computational Fluid Dynamics for Wind Turbine Wake Aerodynamics. *Wind Energy*. 2011;14:799-819.

25. Menter F. R.. Two-Equation Eddy-Viscosity Turbulence Models for Engineering Applications. *American Institute of Aeronautics and Astronautics Journal*. 1994;32(8):1598-1605.

26. Cabezón D., Migoya E., Crespo A.. Comparison of Turbulence Models for the Computational Fluid Dynamics Simulation of Wind Turbine Wakes in the Atmospheric Boundary Layer. *Wind Energy*. 2011;14(7):909-921.

27. El Kasmi A., Masson C.. An Extended Model for Turbulent Flow through Horizontal-Axis Wind Turbines. *Journal of Wind Engineering and Industrial Aerodynamics*. 2008;96(1):103-122.

28. Prospathopoulos J. M., Politis E. S., Rados K. G., Chaviaropoulos P. K.. Evaluation of the Effects of Turbulence Model Enhancements on Wind Turbine Wake Predictions. *Wind Energy*. 2011;14(2):285-300.

29. Abolghasemi M. A., Piggott M. D., Spinneken J., Viré A., Cotter C. J., Crammond S.. Simulating Tidal Turbines with Multi-Scale Mesh Optimisation Techniques. *Journal of Fluids and Structures*. 2016;66:69-90.

30. van der Laan M. P., Andersen S. J.. The Turbulence Scales of a Wind Turbine Wake: A Revisit of Extended k-Epsilon Models. *Journal of Physics: Conference Series*. 2018;1037:072001.

31. Jost E., Klein L., Leipprand H., Lutz T., Krämer E.. Extracting the Angle of Attack on Rotor Blades from CFD Simulations. *Wind Energy*. 2018;21(10):807-822.

32. Wimshurst A., Vogel C. R., Willden R. H. J.. Cavitation Limits on Tidal Turbine Performance. *Ocean Engineering*. 2018;152:223-233.

33. Richards P. J., Norris S. E.. Appropriate Boundary Conditions for a Pressure Driven Boundary Layer. *Journal of Wind Engineering and Industrial Aerodynamics*. 2015;142:43-52.

34. McNaughton J., Cao B., Vogel C. R., Willden R. H. J.. Model Scale Testing of Multi-Rotor Arrays Designed to Exploit Constructive Interference Effects. In: ; 2019; Naples, Italy.

35. Johnson K. E.. *Adaptive Torque Control of Variable Speed Wind Turbines*. Technical Report NREL/TP-500-36265: National Renewable Energy LaboratoryGolden, Colorado; 2004.

36. Larsen G. C., Madsen H. Aa., Thomsen K., Larsen T. J.. Wake Meandering: A Pragmatic Approach. *Wind Energy*. 2008;11(4):377-395.

37. Lissaman P.. Energy Effectiveness of Arbitrary Arrays of Wind Turbines. *Journal of Energy*. 1979;3(6):323-328.

38. Katic I., Højstrup J., Jensen N. O.. A Simple Model for Cluster Efficiency. In: :407-410; 1986; Rome, Italy.

39. Gaumond M., Réthoré P.-E., Ott S., Pena Diaz A., Bechmann A., Hansen K. S.. Evaluation of the Wind Direction Uncertainty and Its Impact on Wake Modelling at the Horns Rev Offshore Wind Farm. *Wind Energy*. 2014;17:1169-1178.

40. Glauert H.. Airplane Propellers. In: Berlin Heidelberg: Springer-Verlag 1935 (pp. 167-269).

41. Shen W. Z., Mikkelsen R. F., Sørensen J. N., Bak C.. Tip Loss Corrections for Wind Turbine Computations. *Wind Energy*. 2005;8:457-475.